IEEE INSTRUMENTATION & MEASUREMENT SOCIETY

Received 25 September 2023; accepted 29 October 2023. Date of publication 14 November 2023; date of current version 6 December 2023.
The review of this paper was arranged by Associate Editor Shutao Li.

Digital Object Identifier 10.1109/OJIM.2023.3332344

Discrimination of Cardiac Abnormalities Based on Multifractal Analysis in Reservoir Computing Framework

BASAB BIJOY PURKAYASTHA AND SHOVAN BARMA (Member, IEEE)

Electronics and Communication Engineering Department, Indian Institute of Information Technology Guwahati, Guwahati 781015, India

CORRESPONDING AUTHOR: S. BARMA (e-mail: shovan@iiitg.ac.in)

This work was supported in part by the Department of Physics, Indian Institute of Technology Guwahati (IITG), Assam, India, and in part by IITI DRISHTI CPS Foundation through the NM-ICPS Scheme under Grant TDP-L2M-CF-2023-007.

ABSTRACT This study proposes a multiclass classification technique based on multifractal spectra for different types of cardiac arrhythmias which are associated with irregularity and/or complex dynamics of the heart. Indeed, the degree of complexity of such dynamics is diverse for different states of cardiac condition. Certainly, such physiological responses of the heart dynamics can be discriminated by analyzing electrocardiogram (ECG) signals through different channels. Earlier, ECG-based works for discriminating cardiac arrhythmias consider the heart as a black box system and the analysis is mostly surrounded with time domain statistical averages or spectral analysis. The works ignore one of the key parameters, i.e., the presence of time-localized irregularities which are strongly associated with different kinds of arrhythmias and contribute to subtle variations in the amplitude and shape of the signal dynamical system while analyzing the signal. Therefore, in this work, we proposed a new method based on multifractal analysis to classify different kinds of cardiac conditions. Here, we followed the dynamical systems approach and computed the multifractal spectrum of the embedded phase space structure of the ECG signal. We performed the classification task by an echo state network to reduce the computational burden. For validation, three well-known datasets (Shaoxing Peoples' Hospital dataset, PTB diagnostic ECG database v1.0.0, and 2017 PhysioNet/CinC Challenge dataset) have been considered. The results and analysis show that the proposed method can achieve a maximum accuracy of up to 96%, which is significantly high. Further, an optimum number of channels/leads has also been evaluated in multichannel ECG analysis. The result and analysis reveal that the effectiveness of the model in classifying various categories of cardiac disorders from ECG.

INDEX TERMS Arrhythmia classification, echo state network (ESN), multifractal analysis, multivariate multifractal singularity spectrum, nonlinear dynamics.

I. INTRODUCTION

RECENTLY, new nonlinear dynamical methods are being employed to analyze complex biological systems, in particular human heart and brain [1], [2], [3], [4], [5], [6], [7], [8]. Such methods can be employed in detecting any dysfunction of the whole system or its specific parts as they prominently display the changes in associated physiological signals. For the heart, any cardiac dysfunction causes a reduction in complexities of heart dynamics which can be traced through electrocardiogram (ECG) [2], [3], [4], [6], [7]. In general, the dynamics of the heart in healthy conditions are highly complex. However, for any damage to heart tissue, blockage of heart vessels, electrolyte imbalance, or any other causes, the normal electrical activity of the heart is disrupted. Besides, contribution of some of electromechanical events to the overall dynamics may be ceased or weakened, which results in reduction of overall complexity in cardiac dynamics. The degree of complexity alteration is contingent upon the nature and severity of the underlying cardiac abnormality. Such variations in complexity levels could be useful for comprehending cardiac conditions, like distinguishing normal/abnormal cardiac rhythms [4], [7], [8]. Eventually, the cardiac cycle is controlled by the bioelectrical signals that travel through the heart which is made up

of many interconnected elements (e.g., ionic channels, transporters, etc.). These elements often display a nonlinear dependence on one or more variables, such as transmembrane potential or ion concentration gradients across the cell membrane [2]. Therefore, building an optimum classifier considering the such nonlinear characteristics of cardiac dynamics for discriminating various types of arrhythmias could be a promising tool.

The ECG signal provides an overall response of the heart, which originates due to different electrical and mechanical events at different parts of the heart [7], [8]. The overall dysfunction of the heart or its parts can be identified by analyzing the change in beat-to-beat interval or heart rate variation (HRV) signal [7], [8], [11]. Any subtle variation in the amplitude, shape, and timing of ECG beats can be explained in terms of variations in the underlying dynamics of the heart. It is nonlinear in nature, and cannot be detected by employing conventional linear analysis, like power spectral analysis, short-time Fourier transforms (STFTs), wavelet transform, etc. [7], [8], [11]. For instance, the STFT fails to detect its time irregularities due to low frequency resolution for fixed window size [11]; although, wavelet provides better flexibility in this regard, but, it treats the irregularities as random noise [11]. Therefore, the involvement of nonlinear dynamic methods, particularly, the multifractal analysis might be appropriate for discriminating of different abnormalities of the heart. Multifractal analysis of ECG signal could provide a details description of singularities associated with the signal by quantifying the variations of its regularity in amplitude, shape, or beat period of the signal.

In literature, most of the works have been in line with de-trended fluctuation analysis (DFA) [9], [10], [11] which attempts to find multifractal signature associated with ECG. In DFA, mainly the variability in the scaling of the fluctuations is considered as quantifying parameters. There are very limited attempts to adopt a dynamical systems approach along with multifractal analysis, which could be appropriate in distinguishing nonlinear dynamic cardiac conditions from healthy/unhealthy subjects. In this regard, Shekatkar et al. [7] and Harikrishnan et al. [8] have considered the multifractal properties of the dynamical attractors from the ECG. They did the binary classification by using best-fit parameters which are evaluated from multifractal spectrum. However, the works focused on only binary classifications considering a few numbers of subjects. Besides, they have used a very limited number of parameters from the spectrum which were for a fixed number of channels. Indeed, consideration of the whole spectrum rather than a few limited parameters might be more appropriate as it is integrated with more inherent properties in detail. Further, multichannel analysis is necessary as all the rhythmic variations may not be associated with a certain number of fixed channels. In addition, for verifying the generality of an idea, diverse data with a large number of subjects should be considered.

Now, the choice of classifier could play a crucial role, which can be designed in traditional machine learning (e.g., k-nearest neighbors, support vector machine, etc.) or deep learning (DL) (e.g., convolution neural network (CNN), recurrent neural network (RNN), long-short term memory (LSTM), etc.) framework. The efficiency of the traditional machine learning-based classifiers are highly dependent on the handcrafted feature engineering, while notable classification performance has been achieved by DL [31], [32], [33], [34] which bypasses the manual feature engineering. Therefore, DL-based approach has been aimed to be involved in this study as the whole multifractal spectrum has been considered for feature extraction. However, the DL-based framework has a huge computational bottleneck in terms of resources and computational time. In this context, the reservoir computing (RC) framework which falls in the family of RNN provides a strong simplification to the learning process and reduces the computational bottlenecks to a great extent [21], [22], [23], [24], [25], [26], [27], [28]. One of the key benefits of the RC algorithm is that its training is performed only at the readout stage and the reservoir configuration remains fixed once initialized. One of the variants of the RC is the echo state network (ESN), which possesses a big reservoir of coupled neurons. The ESN principle relies on the idea that a big random expansion of the input vector often makes it easy for a linear model to fit the data for classification or other tasks. The ESN-based paradigm is already widely used for modeling complex temporal sequences and showed notable performance [21], [22], [23], [24], [25], [26], [27], [28]. Therefore, in this work, the ESN-based formwork has been adopted for efficient classification tasks.

In this view, we propose a new method based on multifractal properties of the dynamical attractors of the ECG signal considering the dynamical systems framework of the heart. The multifractal singularity spectrum has been used for discrimination among different kinds of cardiac conditions. A multiclass classification model has been incorporated into the principles of ESN to make the model computationally efficient. The experimental validation has been performed by using three well-known datasets. Several analyses, including multiclass classification, accuracy, the impact of different channels, comparative evaluations with state-of-the-art methods, etc., have been performed. The major contribution of the work has been summarized as follows.

1) Multifractal analysis of ECG considering the dynamical system framework of the heart for discrimination of different heart conditions; in contrast to earlier works where the heart has been assumed as a black box.
2) Consideration of the whole multifractal singularity spectrum to consider all possible parameters, in opposition to the existing works where certain user-defined parameters have been selected.
3) Use of a simplified bidirectional ESN-based model, a resource-friendly RC framework, for classification tasks.

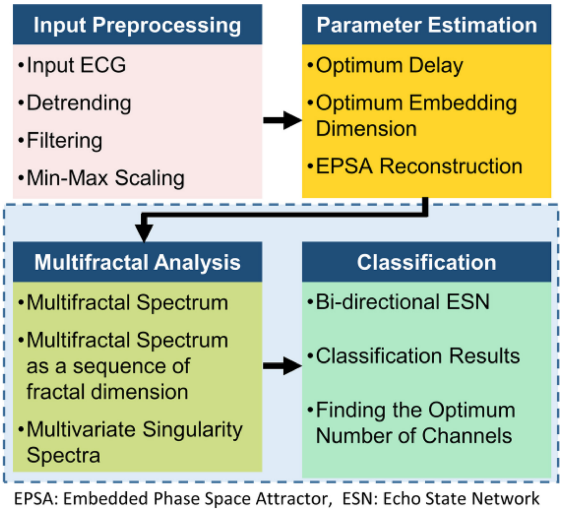

FIGURE 1. System overview of the proposed method.

4) Performing multiclass classification by considering multichannel ECG, in opposition to the existing works where certain fixed channels are taken into account.
5) For validating the generality of the proposed idea, three benchmark datasets are taken into account.
6) The proposed idea has been compared with the state-of-the-art methods.

II. SYSTEM OVERVIEW

In this work, a novel method for classification of different kinds of cardiac abnormalities and normal conditions based on ECG signals has been proposed by exploring the dynamical system framework of the heart. A systematic overview of the proposed method has been illustrated in Fig. 1. It starts with the preprocessing of the raw ECG signal followed by embedded phase space reconstruction. Next, the multifractal analysis of the phase space attractor is constructed to compute the associated multifractal spectra These spectra are fed as input into an ESN-based classifier for discrimination among different types of cardiac conditions (normal/abnormal). Finally, the performance of the proposed model is evaluated in terms of overall accuracy and F1-score. Further, the effectiveness of the idea has been compared with state-of-the-art methods.

III. PROPOSED METHOD

A. PREPROCESSING

The raw ECG signals are always contaminated with different noises and artifacts, which need to be removed for accurate analysis. The presence of any sort of nonlinear trend in ECG may influence the analysis results, especially while statistical methods are involved, which need to be de-trended. It has been accomplished by fitting the data points corresponding to each channel with a polynomial of degree p. Certainly, the optimum value of p is very important as a small value of p may not be able to remove higher-order trends. It has been achieved by computing deviation (δ), the mean square error between the original signal and its fitted version. The deviation δ for any p is expressed in

$$\delta_{(p)} = \frac{1}{N}\sum_{i=1}^{N}\left[x_0(i) - x_p(i)\right]^2 \tag{1}$$

where, $\delta_{(p)}$ is corresponding deviation for a particular p; N is the number of data points in the signal of interest, and (x_0) and x_p refer to original data and fitted signal with a degree p. The noise interference of ECG signals is removed by a Butterworth band-pass filter with a passband of 0.01–250 Hz [11]. Next, the de-trended and filtered signals, c(t), are normalized to 0 and 1 by using min-max scaling, $s(t)$ as

$$s(t) = \frac{C(t) - C_{\min}}{C_{\max} - C_{\min}} \tag{2}$$

where, $c_{\min}$ and $c_{\max}$ are the minimum and maximum values of $c(t)$, respectively.

B. MULTIFRACTAL ANALYSIS

Multifractal analysis has been performed by reconstructing the dynamical attractors of the ECG signal, $s(t)$ in the dynamical systems framework and the multifractal properties have been used to discriminate different types of ECG waveforms. For this purpose, the embedded phase space attractor (EPSA) of the ECG signal has been constructed by computing the optimum delay (τ), which maximizes the predictive power of the input. This follows the computation of the optimum embedding dimension (M) for $s(t)$. The value of τ is calculated by the autocorrelation function of $s(t)$ [19]. The optimum values of M are estimated by following Taken's embedding theorem [20]. Thus, $s(t)$ is embedded into m-dimensional space to reconstruct the EPSA using the delay embedding technique with delays h_τ, where $h = 0, 1, 2, \ldots, (m-1)$. The correlation dimension (D_2) of the reconstructed EPSA is calculated for different values of m ($m = 0, 1, 2, \ldots$) until it is saturated and the optimum value of M is chosen from the saturated values of m [7], [8]. The detailed process of computing D_2 is analogous to the computation of the generalized correlation dimension (D_q) for $q = 2$.

The computation of D_q starts with embedding $s(t)$ to an M-dimensional space using Taken's delay embedding theorem [20] and recreating the phase space structure or embedded attractor of the underlying dynamics using the embedded vector $\widehat{x_i}$

$$\widehat{x_i} = [s(t_i), s(t_i + \tau), \ldots, s(t_i + (M-1)\tau)]. \tag{3}$$

As per Taken's embedding theorem, the phase space structure is the delayed version of the original signal which maintains the same topological properties as that of the original system [20]. For visual intuition, a 2-D projection of the embedded attractor obtained using singular value decomposition (SVD) of $s(t)$ for four different categories of cardiac rhythms has been displayed in Fig. 2. Certain changes in the projection for different types of cardiac rhythms can easily be observed.

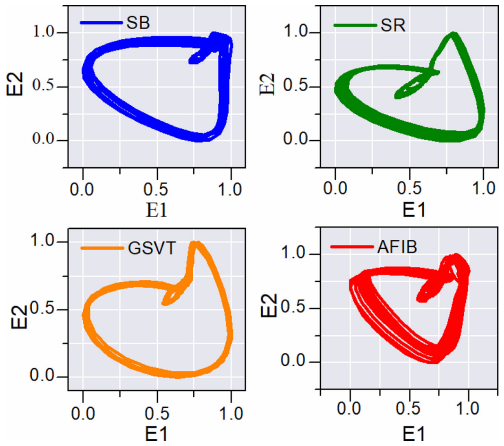

FIGURE 2. 2-D projection of the embedded attractor obtained using SVD transformation of ECG for four different types of cardiac rhythms: SB, SRs, AF, and supraventricular tachycardia (GSVT). The ECG signal, E2 is delayed version of E1 by τ.

The multifractal analysis of EPSA involves calculating the probability of point distribution across the entire EPSA at different scales r. This process begins by calculating the generalized correlation sum $C_q(r)$ as a function of r. The correlation sum $C_q(r)$ quantifies the relative count of data points ($\overrightarrow{x_k}$) within a radius r from specific reference points ($\overrightarrow{x_j}$) chosen as centers within the EPSA. The outcome of this calculation is then raised to the power of $(q-1)$ and averaged across N_c randomly selected centers. This yields the value of the generalized correlation sum

$$C_q(r) = \left[\frac{1}{N_c}\sum_{k=1}^{N_c}\left[\frac{1}{N_v}\sum_{j=1,\, j\neq k}^{N_v} H\left(r - |\overrightarrow{x_k} - \overrightarrow{x_j}|\right)\right]^{(q-1)}\right]^{\frac{1}{(q-1)}} \tag{4}$$

where, H is the Heaviside step function, N_v is the number of data points and q is the generalization parameter. Then the spectrum of generalized correlation can be expressed as

$$D_q = \frac{1}{q-1}\,\frac{\log C_q(r)}{\log r}. \tag{5}$$

In general, D_q is estimated by computing the gradient of $\log C_q(r)$ versus $\log r$ over a region of r for which the gradient remains almost constant. The choice of a range of r to be used for computation is essential as it may yield erroneous D_q values. For the optimum computation of D_q, r should always be confined to the region of the attractor, and it should not extend out of this region. This work utilizes an algorithm as proposed in [8] for evaluation of the optimum value of r and further computation of D_q.

The generalized correlation dimension, D_q, for various values of q quantifies the multifractal nature of the ECG signal. The complexity associated with heart dynamics results in nonuniform distribution of points in the EPSA, which can be measured by calculating the associated singularity spectrum $f(\alpha)$ by Legendre transformation of D_q.

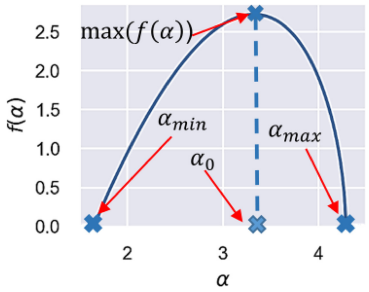

FIGURE 3. Typical $f(\alpha)$ spectrum. The term $(\alpha_{max} - \alpha_{min})$ gives the width of the $f(\alpha)$ spectrum which is the range of multifractal scaling indices.

The $f(\alpha)$ can be expressed as

$$\alpha = \frac{d}{dq}\left[(q-1)D_q\right] \tag{6}$$

$$f(\alpha) = q\alpha - (q-1)D_q. \tag{7}$$

The spectrum of $f(\alpha)$ provides the multifractal signature in terms of interwoven sets with singularity strength α and the corresponding fractal dimension $f(\alpha)$ [8]. However, calculating $f(\alpha)$ directly using (6) and (7) is typically evaded due to the errors that arise during the computation of D_q. These errors render the transformation numerically unfeasible, given that it entails reversing slopes. Hence, we have followed the scheme provided by Harikrishnan et al. [8] to reduce the source of errors. It evaluates an analytical function capable of expressing the typical convex profile of the $f(\alpha)$ spectrum with the help of a set of best-fit parameters (A, $\alpha_{\min}$, $\alpha_{\max}$, γ_1, and γ_2) as expressed

$$f(\alpha) = A(\alpha - \alpha_{\min})^{\gamma_1}(\alpha_{\max} - \alpha)^{\gamma_2}. \tag{8}$$

A typical shape of $f(\alpha)$ spectrum evaluated by (8) has been displayed in Fig. 3. The difference term ($\alpha_{\max}$–$\alpha_{\min}$), i.e., the width of the $f(\alpha)$ spectrum gives the range of multifractal scaling indices, is a measure of the complexities associated with the signal under study. The width increases with the increase in the complexities in the associated signal, γ_1 and γ_2 specify the shape of the $f(\alpha)$ spectrum.

C. MODELING F(α) AS SEQUENCE OF FRACTAL DIMENSION

In our work, the multiclass classification model has been structured considering the whole $f(\alpha)$ spectrum. However, in earlier works, various parameters of the $f(\alpha)$ spectrum including spectrum width, area, or value of α corresponding to the max–min point have been considered for differentiating complexities among various cardiac conditions [17], [18], [19], [20], [21], [22], [23], [24], [25], [26], [27]. Initially, we explored the feasibility of utilizing the width parameter as a discriminating factor among different groups of cardiac conditions; however, the investigation revealed that the width parameter exhibited overlaps among these groups [35]. Therefore, we considered the entire spectrum, which cover all possible features, including those we already know and those we have not fully explored yet. Now, the challenge is to

design a classifier that can learn the complete $f(\alpha)$ spectrum by understanding the sequence of singularity strength α. In this purpose, LSTM can be employed, but it demands huge computational resources [21], [22], [23], [24], [25], [26], [27], [28]. In contrast, RC framework which performs sequence learning. It employs fixed and randomly initialized internal reservoir dynamics, which reduces training complexity, thereby, making it more efficient in dealing with sequential data. More specifically, the ESN-based paradigm, a subtype of RC, is recognized for its proficient handling of complex temporal sequences [21], [22], [23], [24], [25], [26], [27], [28]. However, its effectiveness in learning short-length singularity spectra has not been explored yet. Therefore, we have adopted this RC framework in this work. For efficient use of RC, certain information regarding the representation of the $f(\alpha)$ spectrum is required. The primary requirements are—first, all the $f(\alpha)$ spectrum should be of equal length, corresponding to all the channels, and second all the values of the $f(\alpha)$ spectrum corresponding to each channel for each subject should be sampled at the same sampling interval ($\Delta\alpha$). It is mentioned in [8] that only four ($\alpha_{\min}$, $\alpha_{\max}$, γ_1, and γ_2) out of five parameters involved in (8) are independent and can uniquely characterize the corresponding $f(\alpha)$ spectrum. We have found the deviation of the parameter A is very high, so (8) can be modified by replacing A with a constant C, given by

$$f_1(\alpha) = C(\alpha - \alpha_{\min})^{\gamma_1}(\alpha_{\max} - \alpha)^{\gamma_2}. \tag{9}$$

Now, $f_1(\alpha)$ in (9) can be sampled with some $\Delta\alpha$ for some range of α, such that both $\alpha_{\min}$ and $\alpha_{\max}$ are included in the range. In this process, we obtain a sequence of N samples of $f_1(\alpha)$ corresponding to each channel. As we are interested only in the convex profile of the shape of $f_1(\alpha)$, we modify the $f_1(\alpha)$ sequence by applying the condition $f_1(\alpha) = 0$ for $\alpha < \alpha_{\min}$ or $\alpha > \alpha_{\max}$. Since, in the proposed approach, the ECG records of each subject comprise k sets of ECG recordings corresponding to k channels, the $f_1(\alpha)$'s corresponding to each channel can be merged columnwise to obtain the multivariate singularity spectra (MSS), $f_k(\alpha)$ with shape $[N \times k]$.

D. ESN FOR LEARNING F(α) SPECTRA

A typical ESN comprises of three layers: 1) an input layer; 2) a reservoir layer containing a large number of sparsely connected neurons with recurrent connections; and 3) an output layer (also called the readout layer). Once the ESN is initialized with input, it converts the input into the states of the neurons which guides to prediction of the output. Actually, an ESN learns to couple the output to the neurons. Here, the weights between the input to the reservoir connections and the recurrent connections within the reservoir neurons are carefully chosen and remained fixed throughout the experiment. Only the connection weights between the readout layer and the reservoir are trainable. In this study, we designed an ESN model capable of learning the MSS $f_k(\alpha)$. This model is shown in Fig. 4, where all

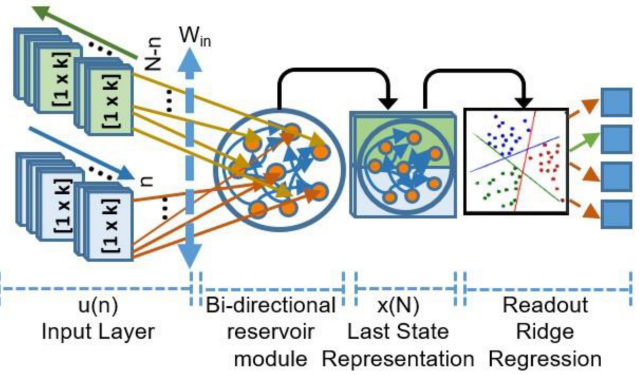

FIGURE 4. Blockwise representation of the proposed ESN framework.

individual blocks are specifically mentioned. The input MSS undergo bidirectional feeding into the input layer, and after modulation through an input scaling matrix (W_{in}), they connect to the reservoir network. The values (weights) of W_{in} are chosen randomly and remain constant throughout the experiment. The recurrent connections among reservoir neurons are determined by the values in W_{res}, which are also randomly chosen and remain unchanged throughout the experiment. With each input instance, the reservoir state is updated, incorporating information from previous instances to uphold the long-state memory characteristic of the network. Ultimately, the final reservoir state, $x(N)$ is obtained for all subjects. As a final unit of our model, a readout unit based on ridge regression is employed to establish a multiclass classification model.

We consider the classification of k-dimensional MSS with N instants of α, whose observation at instant n is denoted as $u(n) \in \mathbb{R}^{1\times k}$. The MSS can be represented in compact form as $N \times k$ matrix $U = [u(1), u(2), \ldots, u(N)]$. The state of the reservoir at instant n of α is $x(n) \in \mathbb{R}^{R\times 1}$, where R is the total number of processing neurons in the recurrent unit (reservoir). $W_{\text{in}} \in \mathbb{R}^{R\times k}$ is the weight of the connections between the input layer and reservoir neurons. $W_{\text{res}} \in \mathbb{R}^{R\times R}$ represents the recurrent connection weights amongst the neurons in the reservoir. We have used the hyperbolic tangent function as nonlinearity in the reservoir units, then the reservoir state equation for modeling sequential data can be given by

$$x(n) = \left[\tanh\left(W_{\text{in}}[u(n)]^T + W_{\text{res}}[x(n-1)\ ]^T\right)\right]^T. \tag{10}$$

The encoder parameters W_{in} and W_{res} are randomly generated and remain fixed throughout the experiment. The generalization competencies of the reservoir mainly depend on five hyper-parameters as detailed in [21]. The reservoir state over different instants of α can be given by $X = [x(1), x(2), \ldots, x(N)]$. All information are required to reconstruct the original input which is embedded into the last state of the reservoir, i.e., $x(N)$, so we took $r_u = x(N)$ as the high-dimensional representation of the input U. Our readout unit is a linear model which is implemented using ridge regression

$$y = g(r_u) = K_0 r_u + k_0 \tag{11}$$

where, $\{K_0, k_0\} = \emptyset_{rd}$ is the decoder parameters, which are adapted by minimizing the ridge regression loss function as given below

$$\emptyset_{\text{rd}} = \frac{1}{2}\|r_u K_0 + k_0 - y\|^2 + \lambda\|K_0\|^2 \tag{12}$$

where, y is a vector containing all the desired output, and the hyperparameter λ controls the weighting of the penalty to the loss function.

In this work, the whole MSS are exposed to the reservoir at once, which facilitates the incorporation of bi-directional data feeding to the same reservoir, both during training and testing to create an improved high-dimensional representation of MSS [28]. The bidirectional architecture of reservoirs has proven to be much more efficient in extracting features from the input sequences [21]. We have realized bi-directionality by exposing the reservoir with the input MSS both from forward and backward directions

$$\begin{aligned}\overrightarrow{x}(n) &= \left[\tanh\left(W_{\text{in}}[u(n)]^T + W_{\text{res}}\left[\overrightarrow{x}(n-1)\right]^T\right)\right]^T \\ \overleftarrow{x}(n) &= \left[\tanh\left(W_{\text{in}}[u(N-n)]^T + W_{\text{res}}\left[\overleftarrow{x}(n-1)\right]^T\right)\right]^T.\end{aligned} \tag{13}$$

The two-state vectors in (13) are concatenated to obtain the full state of the reservoir. Now, with the availability of both recent and past information, dependencies on longer instances can be captured and its last state representation reduces to

$$\bar{x}(N) = M_x^b\left[\overrightarrow{x}(N); \overleftarrow{x}(1)\right] + m_x^b. \tag{14}$$

Now, $[\text{vec}(M_x^b); m_x^b] \in \mathbb{R}^{2R(2R+1)}$ become a representation of r_u. Each MSS is first processed under the same reservoir state to obtain the last state representation of r_u. A detailed description of the implementation of bi-directionality in the reservoir can be found in Bianchi et al. [21].

IV. EXPERIMENTAL METHODOLOGY

A. DATASETS

Shaoxing Peoples' Hospital (SPH) Dataset [18]: The dataset contains 12-lead ECG signals of 10 646 patients categorized under 11 types of heart rhythms, including normal sinus rhythms (SRs) and the rhythms corresponding to different arrhythmias. Each dataset consists of 12 ECGs (one each from 12 leads) of 10-s duration with a sampling frequency of 500 Hz. In this study, we concentrate on four groups: 1) sinus bradycardia (SB); 2) atrial fibrillation (AF); 3) SR; and 4) a combined group containing all records related to various tachycardia cases (GSVT). This consolidation of 11 categories follows the data merging approach outlined in [18] to mitigate category-specific data imbalances in the dataset. Further, 1500 subjects from each of the four groups are randomly chosen as listed in Table 1. Merging the ECG signals to itself five times makes a train and test signal of 50 s.

PTB Diagnostic ECG Database v1.0.0 (PTB): The ECG dataset consists of signals of 78 subjects, which is accessible through the PhysioNet Resource [30]. Out of 78 subjects, 25, 14, and 14 suffer from myocardial infarction, bundle branch block, and cardiomyopathy, respectively; while the rest 25 are from healthy subjects. Each data is collected from 15 channels, but we have considered the conventional 12 leads for analysis. For each data, we have extracted records corresponding to 80 s with a sampling frequency of 1000 Hz.

2017 PhysioNet/CinC Challenge Dataset (PNC-2017) [36], [37]: The dataset consists of 8528 publicly accessible single-lead ECG recordings lasting 30–60 s, sampled at 300 Hz. Among them, 5076 are categorized as normal SR (NSR), 758 fall under AF, 2415 as other rhythms (ORs), and the remaining 279 are classified as noisy data (ND). Train and test data have been divided into 20:80. During the experiment, the training set's imbalance is addressed by replicating records multiple times to approximate the count of the largest group, while the test set remains unchanged.

TABLE 1. Groupings of various rhythm categories for classification.

Merged Groups	Different Rhythm	Number of Subjects	Total Sample
AFIB	AFIB	1055	1500
	AF	445	
GSVT	SVT	348	1500
	AT	121	
	SAAWR	7	
	ST	1000	
	AVNRT	16	
	AVRT	8	
SR	SR	1150	1500
	SI	350	
SB	SB	1500	1500

Note: AF: Atrial Flutter, SVT: Supraventricular Tachycardia, AT: Atrial Tachycardia, SAAWR: Sinus Atrium to Atrial Wandering Rhythm, ST: Sinus Tachycardia, AVNRT: Atrioventricular Node Reentrant Tachycardia, AVRT: Atrioventricular Reentrant Tachycardia, SI: Sinus Irregularity

B. EXPERIMENT

First, in preprocessing, band-pass filtering, de-trending, and max–min scaling have been performed. Eventually, the ECG signal provides an average response of the heart, which arises due to a series of nonlinear processes associated with the underlying dynamics. For the sake of completeness, the statistically rigorous surrogate analysis is conducted to establish the underlying nonlinear and deterministic nature of dynamics encrypted in the ECG signal. For this purpose, surrogates of the ECG have been generated by employing the amplitude adjusted Fourier transform (AAFT) [29]. Next, the correlation dimension (D_2) as a function of embedding dimension (m) has been devised for the original signal and their surrogates as displayed in Fig. 5, in which the horizontal and vertical axes indicate m and D_2, respectively. As seen, the D_2 values of the surrogates deviate significantly from their corresponding values for the original signal, which indicates the encoding of underlying nonlinearity in the signal.

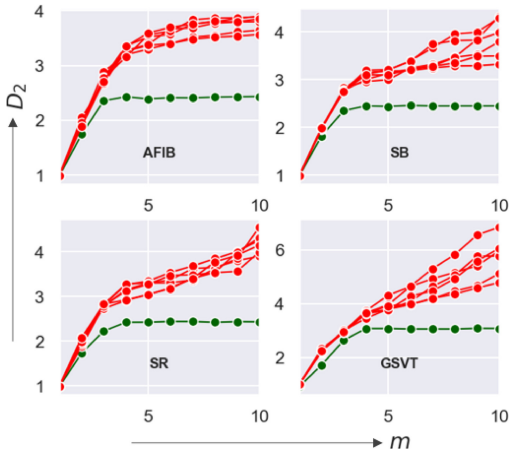

FIGURE 5. Plot for correlation dimension (D_2) as function embedding dimension (m) for the original signal (green) and its AAFT surrogates (red).

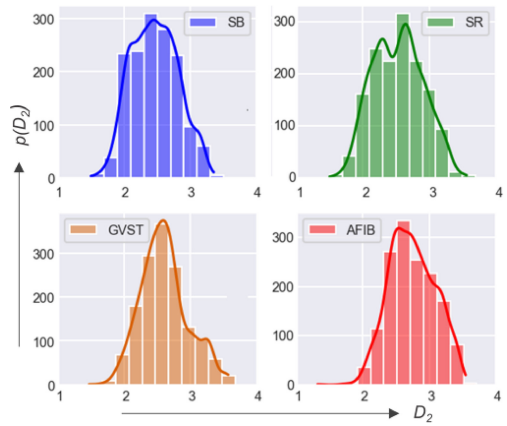

FIGURE 6. Distribution of correlation dimension (D_2) computed with embedding dimension $m = 4$.

Next, for optimum embedding dimension (M), the D_2 is computed for $m = 1, 2, \ldots, 10$ with the delay parameter, τ. Fig. 6 displays the distribution of D_2 corresponding to Channel 1 for $m = 4$ across four distinct cardiac rhythms. In this figure, the horizontal axis represents D_2, while the vertical axis represents $p(D_2)$. As seen, all the D_2 values across all the groups fall below 4, which suggests choosing $m = 4$; hence, $M = 4$. Further, an additional statistic, the channelwise average value of D_2 as a function of m is plotted for all the subjects in Fig. 7, which summarizes that the average D_2 value almost saturates at $M = 4$.

Now, the phase space structure is reconstructed with $M = 4$ following Taken's embedding theorem and D_q has been computed using (4) and (5); where, q values are in the range of $[-20, +20]$, with a step width of $\Delta q = 0.01$. From the D_q spectrum, the $f(\alpha)$ (8) is obtained. The groupwise mean values for all 12 channels are listed in Table 2. Now, the width of the spectrum ($\alpha_{\max}$–$\alpha_{\min}$) is derived which represents a quantitative measure of the complexities of the signal. Certainly, the average value of ($\alpha_{\max}$–$\alpha_{\min}$) from Table 2 shows that the complexity of the heart with SB is maximum, which contradicts the existing study. As per the literature, cardiac abnormalities reduce the complexities associated with heart dynamics [19], [28], [29].

For further analysis, the groupwise distribution of ($\alpha_{\max}$–$\alpha_{\min}$) of the $f(\alpha)$ spectrum for all the subjects has been

TABLE 2. Groupwise mean value for 12 channels.

Channel	Group	γ_1	γ_2	$\alpha_{\min}$	$\alpha_{\max}$
CH 01	SB	0.97±0.07	0.46±0.29	1.38±0.37	3.89±0.29
	SR	0.92±0.14	0.53±0.30	1.62±0.33	3.87±0.35
	GSVT	0.76±0.27	0.52±0.37	1.66±0.39	3.49±0.53
	AFIB	0.91±0.13	0.45±0.28	1.94±0.39	3.67±0.26
CH 02	SB	0.96±0.10	0.50±0.28	1.61±0.31	3.91±0.28
	SR	0.86±0.18	0.56±0.28	1.68±0.29	3.91±0.36
	GSVT	0.67±0.30	0.52±0.36	1.59±0.34	3.39±0.57
	AFIB	0.88±0.15	0.47±0.28	2.02±0.36	3.64±0.29
CH 03	SB	0.93±0.11	0.48±0.29	1.96±0.42	3.85±0.27
	SR	0.88±0.17	0.50±0.32	1.98±0.37	3.76±0.35
	GSVT	0.77±0.27	0.52±0.37	1.72±0.39	3.35±0.63
	AFIB	0.86±0.16	0.44±0.28	2.18±0.37	3.56±0.28
CH 04	SB	0.97±0.08	0.48±0.29	1.51±0.32	3.91±0.25
	SR	0.88±0.18	0.54±0.28	1.65±0.29	3.92±0.38
	GSVT	0.69±0.30	0.51±0.36	1.60±0.34	3.43±0.55
	AFIB	0.88±0.14	0.48±0.28	1.94±0.37	3.61±0.28
CH 05	SB	0.95±0.10	0.46±0.30	1.81±20	3.80±0.33
	SR	0.92±0.15	0.49±0.33	1.86±0.44	3.69±0.36
	GSVT	0.83±0.24	0.50±0.38	1.75±0.45	3.35±0.60
	AFIB	0.88±0.15	0.44±0.28	2.10±0.39	3.59±0.29
CH 06	SB	0.94±0.10	0.47±0.27	1.74±0.37	3.89±0.27
	SR	0.85±0.19	0.52±0.29	1.84±0.32	3.87±0.34
	GSVT	0.71±0.29	0.52±0.36	1.65±0.36	3.40±0.59
	AFIB	0.86±0.16	0.46±0.29	2.13±0.36	3.55±0.30
CH 07	SB	0.89±0.14	0.54±0.24	1.79±0.28	4.10±0.25
	SR	0.85±0.18	0.53±0.28	1.84±0.31	3.94±0.34
	GSVT	0.80±0.25	0.53±0.36	1.63±0.39	3.42±0.63
	AFIB	0.84±0.17	0.48±0.28	2.11±0.33	3.56±0.28
CH 08	SB	0.95±0.10	0.54±0.24	1.47±0.26	4.05±0.30
	SR	0.90±0.16	0.53±0.27	1.53±0.30	3.89±0.36
	GSVT	0.80±0.26	0.57±0.36	1.38±0.34	3.38±0.61
	AFIB	0.89±0.13	0.52±0.27	1.77±0.33	3.58±0.31
CH 09	SB	0.95±0.10	0.54±0.24	1.42±0.26	4.05±0.32
	SR	0.90±0.16	0.55±0.26	1.47±0.28	3.90±0.37
	GSVT	0.75±0.27	0.58±0.34	1.37±0.33	3.52±0.55
	AFIB	0.87±0.14	0.53±0.26	1.68±0.28	3.72±0.28
CH 10	SB	0.95±0.11	0.52±0.25	1.46±0.26	4.04±0.30
	SR	0.89±0.17	0.56±0.27	1.51±0.29	3.91±0.36
	GSVT	0.74±0.26	0.56±0.34	1.39±0.32	3.57±0.54
	AFIB	0.86±0.14	0.54±0.25	1.68±0.28	3.78±0.27
CH 11	SB	0.95±0.10	0.52±0.27	1.52±0.29	4.01±0.27
	SR	0.89±0.17	0.53±0.28	1.57±0.31	3.90±0.36
	GSVT	0.73±0.27	0.54±0.34	1.46±0.33	3.61±0.51
	AFIB	0.85±0.15	0.55±0.25	1.76±0.28	3.81±0.26
CH 12	SB	0.95±0.11	0.50±0.27	1.62±0.32	3.99±0.25
	SR	0.90±0.17	0.56±0.29	1.69±0.33	3.91±0.33
	GSVT	0.74±0.28	0.54±0.35	1.61±0.37	3.60±0.51
	AFIB	0.85±0.15	0.51±0.25	1.89±0.29	3.78±0.25

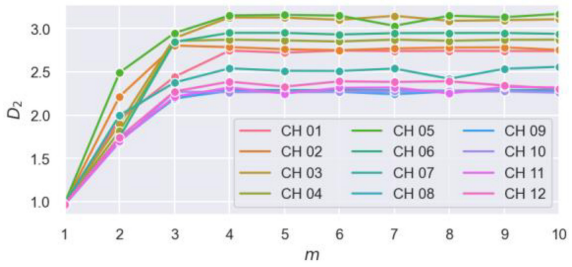

FIGURE 7. Channelwise average value of D_2 as a function of m.

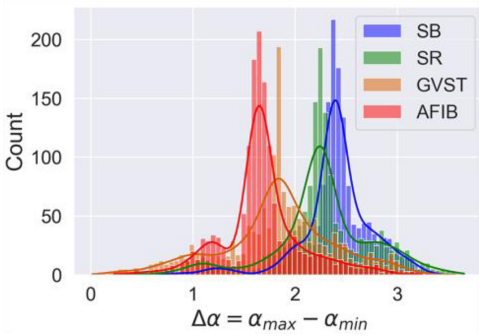

FIGURE 8. Groupwise distribution of this width parameter ($\alpha_{max} - \alpha_{min}$) of $f(\alpha)$ spectrum for all the subjects.

plotted as shown in Fig. 8. As seen, the distributions of four groups overlap each other which shows its insufficiency in discriminating among the groups and for building a multiclass classification model. Another parameter, α_0 that corresponds to maximum values of $f(\alpha)$ (see Fig. 3) is also found to be insufficient as a suitable parameter for multiclass classification. A few scatter plots in Fig. 9 have been displayed corresponding to parameter planes ($\alpha_{\max}$–$\alpha_{\min}$) versus α_0, $\alpha_{\min}$ versus γ_1, $\alpha_{\max}$ versus γ_2, and ($\alpha_{\max}$ versus $\alpha_{\min}$) to observe whether any combination could provide a suitable discriminative feature. As seen, there is no such significant groupwise clustering of data points for the different parameter planes.

Now, an ESN-based classification model that is trained and tested with complete $f(\alpha)$ values corresponding to singularity strength α has been considered. To satisfy the requirements of the ESN, $f_1(\alpha)$ in (9) is sampled for $\alpha = [0: 0.01: 6]$, with $\Delta\alpha = 0.01$, to obtain 600 samples of $f_1(\alpha)$ corresponding to each channel for each subject. Following $\alpha_{\max}$ to be 4.35 (8), the upper bound of α is kept as 6 for "safe" computation. With this, the shape of MSS corresponding to each subject and for k number of channels becomes [600 $\times$ k]. To visualize the $f(\alpha)$ spectrum, mean parameters from Table 2 for specific channels are used and corresponding spectra is illustrated in Fig. 10. As seen, each of the groups can be clearly distinguished.

Next, the performance of the ESN is evaluated for different shapes of MSS for different combinations of channels. For instance, for the SPH dataset, we examine MSS with dimensions of [600 $\times$ k] (where, k refers to number of channels). With $k = 12$, the $f(\alpha)$ spectrum of all 12 channels,

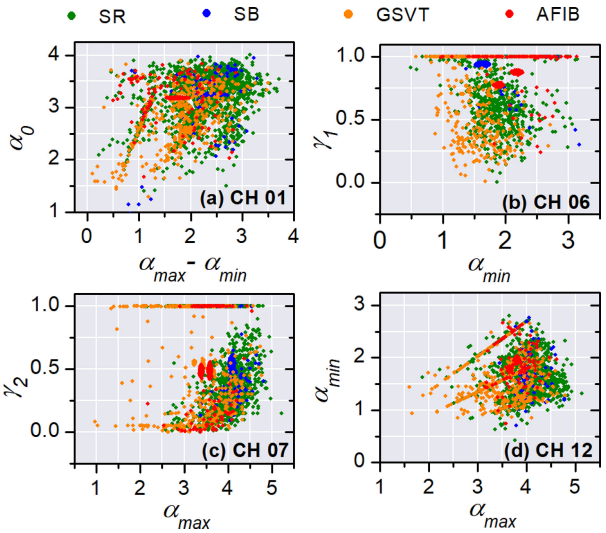

FIGURE 9. Scattered plots for observing discriminative feature in different parametric plans for different channels. (a) (α_{max}–α_{min}) versus α_0 for Channel 1; (b) α_{min} versus γ_1 for Channel 6; (c) α_{max} versus γ_2 for Channel 7; and (d) α_{max} versus α_{min} for Channel 12.

TABLE 3. ESN configuration in terms of hyperparameters.

Parameter	Value
Number of neurons in the reservoir	400
Input scaling (W_{in})	0.1
Sparsity parameter (β)	0.15
Spectral radius (ρ)	0.59
Noise in the reservoir state update	0.01
Leakage in the reservoir state update	0.6
Linear readout hyperparameters (ridge)	5.0

the MSS shape becomes [600 $\times$ 12]. This assessment is repeated multiple times for different values of k (spanning from 12 down to 1). During each experiment, the train and test dataset has been kept at 80:20. The hyperparameters for the proposed ESN with bidirectional capability are tabulated in Table 3. Further, similar experiments have been conducted for all the dataset individually. The classification performance of the model has been evaluated by measuring accuracy and F1 scores.

V. RESULTS AND DISCUSSIONS

The classification performance of the proposed ESN has been evaluated by measuring accuracy for different shapes of the input MSS, i.e., considering different numbers of channels and the results have been displayed in Fig. 11. As seen, there is a significant gain in the performance in terms of accuracy with an increase in the number of channels till 6 (Ch 6, 7, 8, 9, 10, and 11) for the SPH dataset. However, for the *PTB* dataset, all six chest leads are found optimum. Therefore, the observation infers that the optimum number of channels/leads can be six while considering the MSS. Our proposed model achieved peak performance, boasting a maximum accuracy of 96.4% with an F1 score of 0.964 when using the SPH dataset. The corresponding confusion matrix is depicted in Fig. 12.

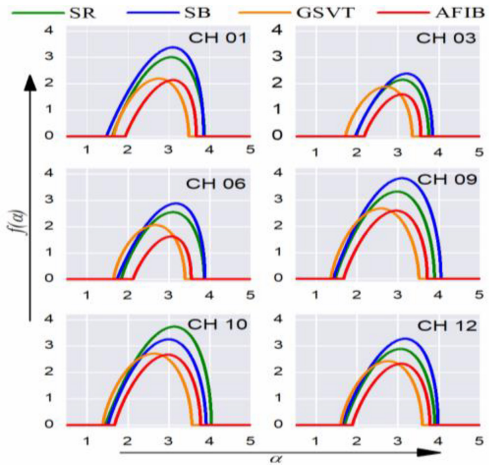

FIGURE 10. $f(\alpha)$ spectrum computed using a groupwise mean of all the parameters. We can clearly distinguish between the spectrums corresponding to the four groups.

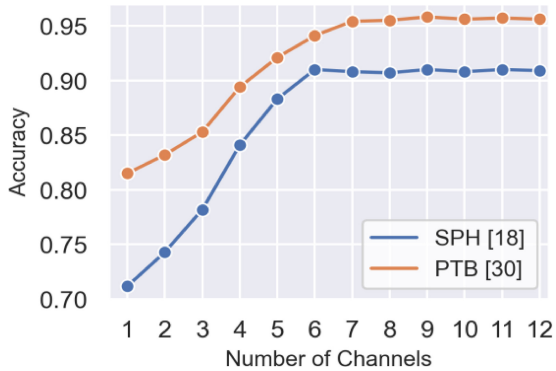

FIGURE 11. Average performance of the ESN in terms of accuracy including different numbers of channels in the input MSS.

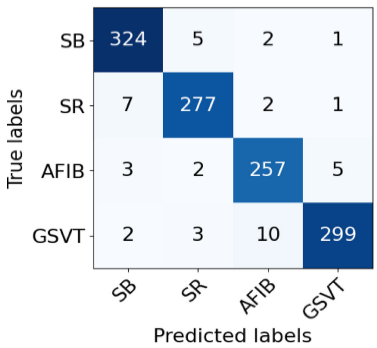

FIGURE 12. Performance of the ESN in terms of accuracy including different numbers of channels in the input MSS.

Further, a comparative study has been performed with the state-of-the-art DL-based techniques and the results have been summarized in Table 4. The analysis reveals that our proposed method outperforms the existing methods in terms of sensitivity and computation time, boasting an exceptional level of accuracy closely aligned with other DL methodologies, including CNN, MLP, and LSTM, as well as their combinations [31], [32], [33], [34]. In a single CPU baseline implementation, executed in an environment with an Intel Core i7-4700MQ processor clocked at 2.4 GHz. The average computation time per beat has been 16.19 ms for our proposed method while the existing method required 21.2 ms [31] (implemented in the same computational environment). It is worth noting that the studies in [32], [33], and [34] employ GPU-based implementations, rendering direct computation time comparisons unfeasible due to disparities in computational environments. Indeed, based on the fundamental principle of DL and reservoir computer framework, our methods required less computational resources as its readout stage works on simple regression problems without involving any back-propagation and gradient decent-based weight correction process. Thus, the proposed idea has been very efficient in terms of showing the best performance but utilizing limited sources.

TABLE 4. Performance comparison with few other works.

Works	Methodology	Type	Accuracy	Recall	CT/Beat
[31]	1D-CNN (2)	Multiclass	**0.990**	0.93	21.2 ms
[32]	Deep CNN (7)	Multiclass	0.913	0.83	-
[33]	CNN (2)+LSTM (3)	Multiclass	0.957	**0.95**	-
[34]	u-MDFA+bi-LSTM	Multiclass	0.973	0.77	-
[7]	MFEA+SVC	Binary	0.90	-	-
Proposed	**MSSEA+ESN**	**Multiclass**	0.964	**0.95**	**16.19 ms**

Note: MFEA: Multifractal features of embedded attractor; MSSEA: Multifractal Singularity Spectra of embedded attractors., CT: Computation.

TABLE 5. Performance comparison with CinC-2017 challenge top performers.

Works	F1 Scores on Validation Dataset					CT (ms)
	NSR	AF	OR	ND	Overall	
S. Datta *et al.* (Rank 1) [39]	0.98	0.96	0.95	0.86	0.961	651
S. Hong *et al.* (Rank 1) [40]	0.97	0.96	0.94	0.86	0.958	828
Proposed	**0.98**	**0.97**	**0.95**	**0.85**	**0.964**	**623**

Furthermore, the study includes a comparison with single-lead, short-length ECG recordings, which offer significant potential for cost-effective and remote diagnostic monitoring solutions. In this purpose, we selected two top-performing approaches from the 2017 PhysioNet/CinC Challenge dataset (PNC-2017) [38], [39] and analyzed their performance and computation time in relation to our proposed model. We evaluated performance using a validation dataset from the PNC-2017 archive, employing the same computational environment with an Intel Core i5-10400 CPU @ 2.90GHz and 16 GB RAM. The results are presented in Table 5. It is clearly seen that our proposed model exhibited impressive efficacy, achieving an overall $F1$ score of 0.964, which is higher, while utilizing less computational time. Hence, our model demonstrates its superiority by delivering high classification performance with minimal computational demands.

VI. CONCLUSION

In this work, we have verified that the multifractal singularity spectrum derived from the embedded attractor of the ECG signal provides a quantitative measure of the complexities associated with cardiac dynamics. A nonlinear

dynamical study is an efficient tool for extracting multifractal signatures from the ECG signal. We have demonstrated a classification technique capable of learning multivariate multifractal singularity spectra. The idea is derived from the ESN-based model, a variant of the RC technique used for studying time series problems. We have found that our model is very efficient in classifying various categories of cardiac disorders when trained with the multifractal singularity spectra associated with the embedded attractor reconstructed out of the ECG signal. We have used two datasets to validate the proposed idea. The results show that the proposed method achieved a classification accuracy of up to 96%. In a comparative study, the proposed technique demonstrates its superiority in terms of low computational complexity but high accuracy.

REFERENCES

[1] M. B. Khodabakhshi and S. Valiallah, "A nonlinear dynamical approach to analysis of emotions using EEG signals based on the Poincare map function and recurrence plots," *Biomed. Tech. (Berl)*, vol. 65, no. 5, pp. 507–520, 2020, doi: 10.1515/bmt-2019-0121.

[2] T. Krogh-Madsen and D. J. Christini, "Nonlinear dynamics in cardiology," *Annu. Rev. Biomed. Eng.*, vol. 14, pp. 179–203, Aug. 2012, doi: 10.1146/annurev-bioeng-071811-150106.

[3] S. K. Nayak, A. Bit, A. Dey, B. Mohapatra, and K. Pal, "A review on the nonlinear dynamical system analysis of electrocardiogram signal," *J. Healthc. Eng.*, vol. 2018, Art. no. 6920420, 2018 doi: 10.1155/2018/6920420.

[4] A. Karma, "Physics of cardiac arrhythmogenesis," *Annu. Rev. Condens. Matter Phys.*, vol. 4, pp. 313–337, Apr. 2013.

[5] B. Akbarian and A. Erfanian, "Automatic seizure detection based on nonlinear dynamical analysis of EEG signals and mutual information," *Basic Clin. Neurosci.*, vol. 9, no. 4, pp. 227–240, 2018, doi: 10.32598/bcn.9.4.227.

[6] Z. Qu, G. Hu, A. Garfinkel, and J. N. Weiss, "Nonlinear and stochastic dynamics in the heart," *Phys. Rep.*, vol. 543, no. 2, pp. 61–162, 2014.

[7] S. M. Shekatkar, Y. Kotriwar, K. P. Harikrishnan, and G. Ambika, "Detecting abnormality in heart dynamics from multifractal analysis of ECG signals," *Sci. Rep.*, vol. 7, Nov. 2017, Art. no. 15127, doi: 10.1038/s41598-017-15498-z.

[8] K. P. Harikrishnan, R. Misra, G. Ambika, and R. E. Amritkar, "Computing the multifractal spectrum from time series: An algorithmic approach," *Chaos.*, vol. 19, no. 4, Art. no. 043129, 2009.

[9] E. Gospodinova, P. Lebamovski, and M. Gospodinov, "Automatic analysis of ECG signals based on their fractal and multifractal properties," in *Proc. Int. Conf. Comp. Syst. Technol. (CompSysTech 21)*, 2021, pp. 136–140, doi: 10.1145/3472410.3472421.

[10] E. Rodriguez, C. Lerma, J. C. Echeverria, and J. A.-Ramirez, "ECG scaling properties of cardiac arrhythmias using detrended fluctuation analysis," *Physiol. Meas.*, vol. 29, no. 11, pp. 1255–1266, 2008, doi: 10.1088/0967-3334/29/11/002.

[11] H. M. M. Cleetus and D. Singh, "Multifractal application on electrocardiogram," *J. Med. Eng. Technol.*, vol. 38, no. 1, pp. 55–61, 2014, doi: 10.3109/03091902.2013.849298.

[12] X. Yang, Z. Wang, A. He, and J. Wang, "Identification of healthy and pathological heartbeat dynamics based on ECG-waveform using multifractal spectrum," *Physica A Stat. Mech. Appl.*, vol. 559, Dec. 2020, Art. no. 125021, doi: 10.1016/j.physa.2020.125021.

[13] A. Gavrovska, G. Zajić, I. Reljin, and B. Reljin, "Classification of prolapsed mitral valve versus healthy heart from phonocardiograms by multifractal analysis," *Hindawi Publ. Corporation*, vol. 2013, no. 376152, 2013, Art. no. 376152, doi: 10.1155/2013/376152.

[14] D. Zhang, C. Wang, C. Li, and W. Dai, "Multi-fractal detrended fluctuation half-spectrum analysis of HRV," *J. Eng.*, vol. 2019, no. 22, pp. 8315–8318, 2019, doi: 10.1049/joe.2019.1067.

[15] A. M. Aguilar Molina, R. I. Rojas Jiménez, and A. M. Diosdado, "Multifractal analysis of ECG time series of stress tests in healthy subjects," *AIP Conf. Proc.*, vol. 2090, no. 1, Apr. 2019, doi: 10.1063/1.5095916.

[16] D. Jiao, Z. Wang, J. Li, F. Feng, and F. Hou, "The chaotic characteristics detection based on multifractal detrended fluctuation analysis of the elderly 12-lead ECG signals," *Physica A Stat. Mech. Appl.*, vol. 540, Feb. 2020, Art. no. 123234, doi: 10.1016/j.physa.2019.123234.

[17] C. Chen et al., "Complexity change in cardiovascular disease," *Int. J. Biol. Sci.*, vol. 13, no. 10, pp. 1320–1328, 2017, doi: 10.7150/ijbs.19462.

[18] J. Zheng, J. Zhang, S. Danioko, H. Yao, H. Guo, and C. Rakovski, "A 12-lead electrocardiogram database for arrhythmia research covering more than 10,000 patients," *Sci Data*, vol. 7, no. 1, p. 48, 2020, doi: 10.1038/s41597-020-0386-x.

[19] K. P. Harikrishnan, R. Misra, G. Ambika, and A. K. Kembhavi, "A non-subjective approach to the GP algorithm for analysing noisy time series," *Physica D Nonlin. Phenom.*, vol. 215, no. 2, pp. 137–145, 2006.

[20] F. Takens, *Dynamical Systems and Turbulence* (Lecture Notes in Mathematics), vol. 898, New York, NY, USA: Springer-Verlag, 1981, pp. 366–381.

[21] F. M. Bianchi, S. Scardapane, S. Løkse, and R. Jenssen, "Reservoir computing approaches for representation and classification of multivariate time series," *IEEE Trans. Neural Netw. Learn. Syst.*, vol. 32, no. 5, pp. 2169–2179, May 2021, doi: 10.1109/TNNLS.2020.3001377.

[22] Y. Zhong, J. Tang, X. Li, B. Gao, H. Qian, and H. Wu, "Dynamic memristor-based reservoir computing for high-efficiency temporal signal processing," *Nat Commun.*, vol. 12, no. 1, p. 408, 2021. doi: 10.1038/s41467-020-20692-1.

[23] D. J. Gauthier, E. Bollt, A. Griffith, and W. A. S. Barbosa, "Next generation reservoir computing," *Nat. Commun.*, vol. 12, 2021, Art. no. 5564, doi: 10.1038/s41467-021-25801-2.

[24] H. T. Fan, W. Wang, and Z. Jin, "Performance optimization of echo state networks through principal neuron reinforcement," in *Proc. Int. Joint Conf. Neural Netw. (IJCNN)*, 2017, pp. 1717–1723, doi: 10.1109/IJCNN.2017.7966058.

[25] W. Aswolinskiy, R. F. Reinhart, and J. Steil, "Time series classification in reservoir and model-space: A comparison," in *Proc. Workshop Artif. Neural Netw. Pattern Recognit. (IAPR)*, 2016, pp. 197–208.

[26] T. Kim and B. R. King, "Time series prediction using deep echo state networks," *Neural Comput. Appl.*, 2020, pp. 17769–17787. doi: 10.1007/s00521-020-04948-x.

[27] Z. Li and G. Tanaka, "Multi-reservoir echo state networks with sequence resampling for nonlinear time-series prediction," *Neurocomputing*, vol. 467, pp. 115–129, Jan. 2022, doi: 10.1016/j.neucom.2021.08.122.

[28] F. M. Bianchi, S. Scardapane, S. Løkse, and R. Jenssen, "Bidirectional deep-readout echo state networks," in *Proc. Eur. Symp. Artif. Neural Netw.*, 2018, pp. 425–430.

[29] J. Theiler, S. Eubank, A. Longtin, B. Galdrikian, and J. D. Farmer, "Testing for nonlinearity in time series: The method of surrogate data," *Physica D Nonlin. Phenom.*, vol. 58, nos. 1-4, pp. 77–94, 1992.

[30] A. L. Goldberger et al., "PhysioBank, PhysioToolkit, and PhysioNet: Components of a new research resource for complex physiologic signals," *Circulation*, vol. 101, no. 23, pp. e215–e220, 2000.

[31] S. Kiranyaz, T. Ince, and M. Gabbouj, "Real-time patient-specific ECG classification by 1-D convolutional neural networks," *IEEE. Trans. Biomed. Eng.*, vol. 63, no. 3, pp. 664–675, Mar. 2016, doi: 10.1109/TBME.2015.2468589.

[32] Ö. Yildirim, P. Pławiak, R. S. Tan, and U. R. Acharya, "Arrhythmia detection using deep convolutional neural network with long duration ECG signals," *Comput. Biol. Med.*, vol. 102, pp. 411–420, Nov. 2018, doi: 10.1016/j.compbiomed.2018.09.009.

[33] J. H. Tan et al., "Application of stacked convolutional and long short-term memory network for accurate identification of CAD ECG signals," *Comput. Biol. Med*, vol. 94, pp. 19–26, Mar. 2018, doi: 10.1016/j.compbiomed.2017.12.023.

[34] B. Ganguly, A. Ghosal, A. Das, D. Das, D. Chatterjee, and D. Rakshit, "Automated detection and classification of arrhythmia from ECG signals using feature-induced long short-term memory network," *IEEE Sens. Lett.*, vol. 4, no. 8, pp. 1–4, Aug. 2020, doi: 10.1109/LSENS.2020.3006756.

[35] B. B. Purkayastha, A. Hazarika, A. Thomas, and S. Poddar, "Cardiac anomaly detection using embedded attractors reconstructed from multichannel ECG," in *Proc. Int. Conf. Biomed. Bioinform. Eng. (ICBBE '22)*, 2023, pp. 120–126, doi: 10.1145/3574198.3574217.

[36] G. D. Clifford et al., "AF classification from a short single lead ECG recording: The PhysioNet/computing in cardiology challenge," in *Proc. IEEE Comput. Cardiol. (CinC)*, 2017, pp. 1–4, doi: 10.22489/CinC.2017.065-469.

[37] A. L. Goldberger et al., "PhysioBank, PhysioToolkit, and PhysioNet: Components of a new research resource for complex physiologic signals, *Circulation*," vol. 101, no. 23, pp. e215–e220, 2000.

[38] S. Datta et al., "Identifying normal, AF and other abnormal ECG rhythms using a cascaded binary classifier," in *Proc. Comput. Cardiol.* 2017, pp. 1–4, doi: 10.22489/CinC.2017.173-154.

[39] S. Hong et al., "ENCASE: An ENsemble ClASsifiEr for ECG classification using expert features and deep neural networks," in *Proc. Comput. Cardiol. (CinC)*, 2017, pp. 1–4, doi: 10.22489/CinC.2017.178-245.

BASAB BIJOY PURKAYASTHA received the M.Sc. degree in electronic sciences and the M.Tech. degree in communication technologies from Gauhati University, Guwahati, India, in 2002 and 2012, respectively. He is currently pursuing the Ph.D. degree from the Indian Institute of Information Technology Guwahati, Guwahati, India.

He is currently working as a Technical Officer Gr-II with the Department of Physics, Indian Institute of Technology Guwahati.

SHOVAN BARMA (Member, IEEE) received the M.Tech. degree in VLSI design from the Indian Institute of Engineering Science and Technology Shibpur, Howrah, India, in 2008, and the Ph.D. degree in electrical engineering VLSI design from National Cheng Kung University, Tainan, Taiwan, in 2015.

He has been an Associate Professor with the Indian Institute of Information Technology Guwahati, Guwahati, India, since 2016.